Development of a Human Neuromuscular Tissue-on-a-Chip Model on a 24-Well-Plate-Format Compartmentalized Microfluidic Device

Kazuki Yamamoto[1], Nao Yamaoka[1], Yu Imaizumi[1], Takunori Nagashima[1], Taiki Furutani[1], Takuji Ito[2], Yohei Okada[2], Hiroyuki Honda[1], Kazunori Shimizu[1*]

[1] *Department of Biomolecular Engineering, Graduate School of Engineering, Nagoya University, Nagoya, Aichi, Japan*

[2] *Department of Neurology, Aichi Medical University School of Medicine, Nagakute, Aichi, Japan*

*E-mail: shimizu@chembio.nagoya-u.ac.jp

Keywords: organ-on-a-chip, motor neurons, skeletal muscle cells, neuromuscular junctions, phenotypic screening

Abstract

Engineered three-dimensional models of neuromuscular tissues are promising for use in mimicking their disorder states *in vitro*. Although several models have been developed, it is still challenging to mimic the physically separated structures of motor neurons (MNs) and skeletal muscle (SkM) fibers in the motor units *in vivo*. In this study, we aimed to develop microdevices for precisely compartmentalized coculturing of MNs and engineered SkM tissues. The developed microdevices, which fit a well of 24 well plates, had a chamber for MNs and chamber for SkM tissues. The two chambers were connected by microtunnels for axons, permissive to axons but not to cell bodies. Human iPSC (hiPSC)-derived MN spheroids in one chamber elongated their axons into microtunnels, which reached the tissue-engineered human SkM in the SkM chamber, and formed functional neuromuscular junctions with the muscle fibers. The cocultured SkM tissues with MNs on the device contracted spontaneously in response to spontaneous firing of MNs. The addition of a neurotransmitter, glutamate, into the MN chamber induced contraction of the cocultured SkM tissues. Selective addition of tetrodotoxin or vecuronium bromide into either chamber induced SkM tissue relaxation, which could be explained by the inhibitory mechanisms. We also demonstrated the application of chemical or mechanical stimuli to the middle of the axons of cocultured tissues on the device. Thus, compartmentalized neuromuscular tissue models fabricated on the device could be used for phenotypic screening to evaluate the cellular type specific efficacy of drug candidates and would be a useful tool in fundamental research and drug development for neuromuscular disorders.

1. Introduction

The physical movement of the body is induced by the transmission of signals to the motor units, consisting of motor neurons (MNs) and skeletal muscle (SkM) fibers. MNs whose cell body is in the spinal cord elongate the axon to the SkM fibers. The terminals of axons form neuromuscular junctions (NMJs), chemical synapses, with muscle fibers. When an action potential reaches the terminal of the axon, acetylcholine is released from the axon terminal and binds to the acetylcholine receptors (AChRs) on the muscle fiber membrane, inducing muscle contraction (1, 2). Neuromuscular disorders such as MN diseases, neuropathies, NMJ disorders, and myopathies affect one or more components of the motor unit, causing progressive motility disturbances (3). As neuromuscular disorders span a broad range of rare conditions with diverse genetic and nongenetic etiologies and pathophysiologies, it is particularly challenging to develop comprehensive animal models (4). Thus, it is required to develop more efficient and predictive *in vitro* neuromuscular disorder models to improve our mechanistic knowledge on these disorders and develop effective treatments (4-7).

Engineered three-dimensional (3D) models of neuromuscular tissues are promising for use in mimicking the disorder state *in vitro*. A common approach to fabricate them is to attach/mix the MNs directly to the tissue-engineered SkM (8-13). The usefulness of this approach for modeling of neuromuscular disorders has been demonstrated by showing that the addition of IgG isolated from myasthenia gravis patients, an autoimmune disease of NMJs, reduced the contraction of the innervated tissues (13). However, owing to the attaching/mixing nature of this approach, it is challenging to monitor individual cell types and control their culture conditions.

To overcome this issue, another approach has been proposed where the coculture of MNs and engineered SkM tissues with their cell bodies is physically separated, which mimics the physically

separated structure of MNs and muscle fibers in the motor units (14-17). In the pioneering studies by Kamm et al., microfluidic devices for the formation of compartmentalized motor units were developed (14, 15). MN spheroids and engineered SkM tissues were positioned separately in a microchannel filled with collagen gel. The axons of MNs elongated within the gel reached the muscle tissues and formed NMJs with the muscle fibers in the tissues. The devices have been used to model amyotrophic lateral sclerosis using induced pluripotent stem cells (iPSCs) from patients. This indicates that this approach has the potential for mimicking neuromuscular disorders. However, using the reported devices, it is still challenging to keep all cell bodies of MNs and muscle fibers separated during a culture period and precisely control the culture conditions for each cell type because of the rough compartmentalization by the collagen gel.

Compartmentalized coculture of cell bodies and axons of neurons has been achieved by microfabricated devices with two chambers connected to each other by microtunnels permissive to axons but not to cell bodies (18, 19). Devices with microtunnels have been applied in development of *in vitro* two-dimensional (2D) compartmentalized motor unit models by coculturing MNs and SkM cells in each chamber (20-23). The isolation characteristic of the chambers allows to add drugs or other small molecules to one or both chambers selectively (24). Electrical stimulation can be applied to the cells in each chamber (25). Furthermore, it is possible to apply chemical and/or physical stimulation to the middle of the axons to study axon injury and regeneration (26). Thus, compartmentalization by the microtunnels for axons has been widely accepted as a powerful approach for neuromuscular research.

Generating a contractile force is a primary characteristic of SkM tissues, while the weakening of this contractile force is induced by various neuromuscular disorders. Hence, many methods for measuring the contractile force generated by cultured SkM cells or tissues have been developed

and used for disease research and drug development (27). More recently, Madden et al. reported that the contractile force of engineered human SkM tissues mimicked the clinical responses of SkM to drugs (28). Nesmith et al. reported that the *in vitro* Duchenne muscular dystrophy muscle model failed to achieve the same contractile strength as the *in vitro* healthy muscle model (29). Furthermore, we reported that engineered atrophic SkM tissues on microdevices for measuring the contractile force could be applied to drug screening, by using the contractile force as an indicator (30). Thus, the contractile force is one of the significant factors to be evaluated for the *in vitro* SkM tissue model.

In this study, we propose microdevices for a precisely compartmentalized coculture of MNs and engineered SkM tissues (Fig. 1). We integrated the microtunnels for axons into the previously developed microdevices for a contractile force measurement of the engineered SkM tissues (30-32). The developed microdevices that fit a well of a 24-well plate have two chambers connected by the microtunnels for axons. Human iPSC (hiPSC)-derived MN spheroids in one chamber elongated their axons into microtunnels, which reached the tissue-engineered human SkM in the other chamber, and formed functional NMJs with the muscle fibers. As the cell bodies of the MNs and SkM cells were separated by the microtunnels, we succeeded in controlling the culture conditions of each cell type and applied chemical or physical stimulations to cell bodies or middle of the axons selectively. To the best of our knowledge, this is the first study on microdevices for the fabrication of precisely compartmentalized 3D models of neuromuscular tissues.

2. Materials and Methods

2.1 Materials

SU-8 3005 (Nippon Kayaku, Tokyo, Japan), SU-8 developer (Nippon Kayaku, Tokyo, Japan), polydimethylsiloxane (PDMS; SILPOT 184, DuPont Toray Specialty Materials K.K., Tokyo, Japan), StemFit (AK02N, Ajinomoto, Tokyo, Japan), i-Matrix-511 (381-07363, Fujifilm Wako Chemicals, Osaka, Japan), TrypLE™ Select CTS™ (A12859-01, Thermo Fisher Scientific, Waltham, MA), UltraPure™ 0.5-M EDTA (15575020, Thermo Fisher Scientific), Y-27632 (08945-71, Nacalai Tesque, Kyoto, Japan), fibrinogen (F8630, Sigma-Aldrich), thrombin from bovine plasma (T4648, Sigma-Aldrich, St. Louis, MO), 6-aminocapuroic acid (6-AA, A2504, Sigma-Aldrich), trans-4-(aminomethyl) cyclohexanecarboxylic acid (TA, A0236, Tokyo Chemical Industry, Tokyo, Japan), DMEM (08458-16, Nacalai tesque), Ultroser G serum substitute (15950-017, Pall Corporation, Port Washington, NY, USA), Matrigel® basement membrane matrix (354234, Corning Inc., Corning, NY, USA), Dulbecco's modified Eagle medium/ Nutrient Mixture F-12 (DMEM-F12; 042-30555, Fujifilm Wako Chemicals), pluronic F-127 (low ultraviolet (UV) absorbance) (P6867, Thermo Fisher Scientific), tetrodotoxin (TTX, 206-11071, Fujifilm Wako Chemicals), vecuronium bromide (Vb; 223-01811, Fujifilm Wako Chemicals), Anti α-actinin mouse IgG antibody (A7811, Sigma-Aldrich), CF555A Goat Anti-mouse IgG (H+L), highly cross-absorbed (20231, Biotium, Fremont, CA), RapiClear 1.52 (Sunjin Lab Co., Hsinchu City, Taiwan), were employed.

2.2 Microdevice concept and design

A conceptual illustration of the developed microdevice is shown in Fig. 1A. The microdevice had two chambers: one for engineered SkM tissues and another for MNs (Fig. 1A and B). The SkM tissue chamber developed in our previous studies (30-32) and the MN chamber developed in this study were integrated. As the chambers are separated by the microtunnels for axons, the axons of

MNs seeded into the MN chamber reach the SkM tissues cultured in the SkM chamber (Fig. 1B). The contractile force of the SkM tissues is quantified by measuring the displacement of the tip of the micropost in response to muscle contraction. Two steps of three and nine microtunnels for axons were designed at the tip of the MN chamber (Fig. 1C). To selectively apply chemical or mechanical stimuli to the middle of the axons, the MN chamber had a microchannel for axon stimulation (Fig. 1C).

The SkM chamber consisted of a dumbbell-shaped pocket for tissue formation and two microposts (30). One micropost was attached to the MN chamber and the other was used to measure the contractile force (Fig. 1B). The microposts were designed with a diameter of 500 μm and a height of 4 mm, following our previous study in which the same human SkM myoblasts were used (32). The MN chamber consists of a microchannel for axon elongation, a microchannel for axon stimulation, and microtunnels for axons (Fig. 1C). The microchannel for axon elongation was designed with a height of 60 μm, width of 150 μm, and length of 5000 μm, which is sufficiently long to bridge the micropost and the edge of the dumbbell-shaped pocket. The microtunnels for axons, which were permissive to axons but not to cell bodies, were designed with a height of 3 μm, width of 10 μm, and length of 100 μm, which were comparable to dimensions used in previous studies (19, 21, 22).

2.2 Microdevice fabrication

The MN chamber was fabricated by standard PDMS soft lithography using an SU-8 mold. Micropatterned molds were fabricated by negative photoresist photolithography using SU-8 on a silicon wafer. To fabricate microtunnels for axons with a height of 3 μm, SU-8 3005 was diluted (1:1) with cyclopentanone, spin-coated onto a Si wafer at 3000 rpm for 30 s, and heated at 95 °C

for 10 min. The wafer was then exposed to UV light through a photomask and heated at 95 °C for 10 min. Subsequently, to fabricate microchannels with a height of 60 µm, SU-8 3050 was spin-coated on the silicon wafer with micropatterns at 2000 rpm for 30 s, heated at 95 °C for 1 h, exposed to UV light through a second mask, and then heated at 95 °C for 10 min. The wafers were developed in an SU-8 developer and washed with isopropanol. PDMS (base:catalyst = 10:1) was placed on the mold, spin-coated at 800 rpm for 30 s, and heated at 70 °C for 1 h to fabricate part I (Supplementary Fig. 1). A cylindrical PDMS (diameter: 8 mm, height: 2 mm) (Part II) was attached to Part I by an air plasma treatment, and then the MN seeding port and inlet/outlet for the microchannel for axon stimulation were punched out with biopsy punches with diameters of 2 and 1.5 mm, respectively. After cutting the tip of part I, a part-III cylindrical PDMS (outer diameter: 8 mm, height: 2 mm) with a hole (diameter: 6 mm) was bonded to part II. The assembled parts were then bonded to the PDMS film (thickness of approximately 30 µm) on Si wafers using air plasma. The fabricated MN chamber was bonded onto the chamber for SkM tissues (32). The completed microdevices were exposed to UV light for at least 2 h for sterilization before use for the coculture.

2.3 Cell culture

hiPSC clone (201B7) (33) were provided by Dr. Shinya Yamanaka (RIKEN BRC through the Project for Realization of Regenerative Medicine and National Bio-Resource Project of the MEXT, Japan), and cultured as reported previously (34). hiPSCs were maintained with Stemfit AK02N on an iMatrix-511 coating (0.5 µg/cm^2). MN differentiation of hiPSCs was performed according to a reported method (35). hiPSCs were stripped from the flask with a 1:1 mixture of TrypLE:0.5-mM EDTA. The cells were suspended at 1.0×10^5 cells/mL in AK02N containing 10-µM Y27632 and

seeded into a 6-mm cell culture dish to form spheroids. After the spheroid was formed, the medium was exchanged with embryoid body medium and cultured for 14 days before seeding to the device. Hu5/KD3 is an immortalized human myogenic cell developed by Hashimoto et al. (36). The Hu5/KD3 myoblasts were seeded into collagen-type-I-coated T-75 flasks and cultured at 37 °C under 5% CO_2 and 10% O_2 in DMEM consisting of 20% FBS, 0.5% penicillin–streptomycin, 2 mM of L-glutamine, and 2% Ultroser G serum substitute (GM).

2.4 3D coculture of SkM tissues and MN spheroids on the microdevices

The process for the coculture is shown in Fig. 1D. To prevent adhesion of muscle tissue to the surface of the microdevice, the dumbbell-shaped pockets of the device were filled with a 2% Pluronic solution and incubated for 1 h at 25 °C. After coating, the solution was removed and the entire device was soaked in a Matrigel solution diluted 30-fold by DMEM-F12 and incubated at 25 °C for 3 h to enable MN adhesion onto the surface of the MN chamber. After all solutions were drained, hiPSC-derived MN spheroids with a diameter of 100–200 μm were seeded into the MN seeding port on day −6. The chamber for MNs was filled with a MN medium, while the SkM tissue chamber was filled with GM. On day −4, an SkM tissue was fabricated, according to the reported method (32). A hydrogel containing fibrin, Matrigel, and human SkM myoblasts, Hu5/KD3 myoblasts, were formed by adding 2% thrombin at a volume of 1.6% to the solution, filling a dumbbell-shaped pocket, and incubating at 37 °C for 30 min. GM was replaced with GM with 6-AA and TA to prevent hydrogel degradation. On day −2, the medium was replaced with DMEM containing 2% horse serum, 1% PS, 2 mg of 6-AA, and 1-mg/mL TA (differentiation medium (DM)). The medium was replaced every two or three days. On day 0, the SkM tissues were suctioned using the gel loading tip equipped with the vacuum aspirator and lifted to the top of the

microposts for contact with the tip of the MN chamber. Subsequently, we observed contraction of the SkM tissues for 10 days.

2.5 Evaluation of the contractility of SkM tissues cocultured with MNs

The displacement of the tip of the micropost was observed under an upright microscope (BX53, OLYMPUS, Japan) equipped with ORCA-Spark (Hamamatsu Photonics, Hamamatsu, Japan). The contractile force was calculated using the displacement of the tip using the reported equation (32). For the measurement of contraction of the cocultured SkM tissues induced by spontaneous firing of MNs, the displacement of the tip of the micropost was observed within 5 min after removing the tissues from the 37 °C incubator to avoid the loss of MN activities due to the temperature decrease. To activate the MNs, glutamate was added at 400 μM into the MN chamber. TTX or Vb was added at 2 μM or 20 μM, respectively, into either the SkM chamber or MN chamber, immediately after the addition of glutamate into the MN chamber. PBS was used to dissolve glutamate, TTX and Vb. A motion tracking software (PV Studio 2D, OA Science, Miyazaki, Japan) was used to analyze the movement of the tip of the micropost.

2.6 Region-selective axonal stimulation on the microdevice

The staining solution was prepared by adding 5 μL of Cell Brite™ Membrane Dyes to 1 mL of culture medium. The medium was removed from the microdevice and 7 μL of the staining solution was slowly injected into the inlet of the microchannel for axon stimulation (Fig. 1B). After incubation at 37 °C for 30 min, the microchannel was washed with PBS and observed under a fluorescence microscope (BZ-X700, Keyence).

To denature the axons, shear stress was applied by flowing liquid through the microchannel for

axon stimulation. The tip of the microchip was placed in a close contact with the inlet/outlet of the microfluidic channel and the culture medium was forced to flow (Fig. 1B). The shear stress was calculated as

Shear stress $\tau = (4\mu Q)/(\pi a^3)$,

where μ is the viscosity of the flowing liquid [Pa·s], Q is the volume flow rate [m^3/s], and a is the radius of the channel [m]. As the microchannel is rectangular, the equivalent radius was obtained by dividing the cross-sectional area by the perimeter.

2.7 Immunofluorescence staining

Immunofluorescence staining was performed as reported previously with some modifications (32) . Briefly, the tissue was left in 4% paraformaldehyde for 120 min and permeabilized with 2% PBST (2% Triton X-100 in PBS) and blocked with blocking solution (10% goat serum and 1% Triton X-100 in PBS). The tissue was incubated with the primary antibody. After washing with PBS, it was incubated with secondary antibody. Then, the tissue was clarified using Rapiclear 1.52. Images were obtained by a fluorescence microscope (BZ-X700, Keyence).

3. Results and Discussion

3.1 Cell culture on the fabricated microfluidic devices

The developed device is shown in Fig. 2A. The device was compatible with the well of a commercially available 24-well plate (Fig. 2B). hiPSC-derived MN spheroids were seeded in the MN seeding port in the MN chamber (Fig. 2C). After six days of culturing, the MN elongated the axons in the microchannel (+) and the tips of several axons reached the three microtunnels for axons. After 10 days, the tips of dozens of axons passed through the nine microtunnels for axons

and reached the outside (*) of the MN chamber. No MN cell bodies were observed in the areas of (#) and (*), suggesting that compartmentalized coculturing of MNs and SkM tissues could be achieved using the developed MN chamber. Fig. 2D shows representative images of the coculture on the microdevice in a well of the 24-well plate. The axons were elongated from MN spheroids seeded in the MN chamber and the ribbon-shaped innervated SkM tissue was formed by self-organization (Fig. 2E). Myotubes in the SkM tissues were aligned along the long axis of the tissues (Fig. 2F).

As shown in Fig 2C, the axons in the MN chamber (+) formed a fork-like structure with three tines via the self-assembling of axons after they reached the three microtunnels. We confirmed that the number of tines was consistent with the number of microtunnels using the MN chamber with one step of nine microtunnels for the axon (Supplementary Fig. 2). The structure of the fork handle appeared similar to the structure of the axon fascicle, which was reported as a motor nerve organoid by Kawada et al. (37). They reported that the axons extended from the iPSC-derived MN spheroid in the Matrigel-coated PDMS microchannel (width = 150 μm and height = 150 μm) spontaneously assembled into a unidirectional fascicle and showed that the axon fascicle was electrically active and elastic and could serve as a model to evaluate degeneration of axons *in vitro*. In the present study, we obtained the axon fascicle with tines by using the Matrigel-coated PDMS microchannel (width = 150 μm and height = 60 μm) (Figs. 1C and 2C) and demonstrated the coculture with SkM tissues (Fig. 2D). To the best of our knowledge, a coculture of the axon fascicle and SkM tissues *in vitro* has not been reported thus far. Although further studies are needed to investigate the properties of axon fascicles with a fork-like structure, we believe that the developed compartmentalized microfluidic device will enable, for the first time, a platform to model nerve-muscle interaction.

3.2 Selective stimulation of the middle of the axons of the MNs cultured in the MN chamber

We evaluated whether chemical or mechanical stimulation could be applied selectively to the axons of the MNs elongated in the microchannel for axon stimulation of the MN chamber. MN spheroids were seeded into the MN seeding port and cultured until their axons reached the outside of the MN chamber. For the chemical stimulation, 7 μL of the medium mixed with Cell Brite™ cytoplasmic membrane dye was injected slowly into the microchannel for axon stimulation (#) (Fig. 3A). After 30 min, the fluorescently stained axons were observed in the area (#), whereas the axons in the area (+) were not stained (Fig. 3B). These results suggest that selective chemical stimulation was possible. For the mechanical stimulation, 200 μL of the medium was injected at a shear stress of 60 Pa into the microchannel for axon stimulation (#) (Fig. 3C). The elongated axons in the area (#) disappeared after the application of the shear stress for 30 s, whereas the axons in the area (+) remained as they were (Fig. 3D). Notably, the axons reelongated in the area (#) after 24 h of stimulation, which suggests a possible application of the developed coculture microdevice to model the axon injury and regeneration (Fig. 3E). These results indicate that mechanical stimuli can be applied selectively to the axons of the MN in the microchannel for axon stimulation in the MN chamber.

3.3 Time course trend of spontaneous contraction of engineered SkM tissues cocultured with MN spheroids on the device

We cocultured MN spheroids and engineered SkM tissues on the device. SkM myotubes innervated with MNs exhibited spontaneous contraction in response to spontaneous firing of MNs

(38). Thus, we analyzed the spontaneous contraction of the SkM tissues cocultured with MN spheroids on the devices.

Fig. 4A shows the appearance of the cocultured SkM tissues on the device on days 0, 4, and 8. The tip of the micropost was gradually pulled toward the MN chamber by increasing the passive tension (Fig. 4B). The passive tension of the cocultured SkM tissue was significantly larger than that of the monocultured SkM tissue. Fig. 4C shows the displacement of the tip of the micropost moved by the spontaneous contraction of the SkM tissue on days 4, 6, and 8. The SkM tissue contracted periodically at approximately 2 Hz on days 4 and 6 and nonperiodically on day 8 (Supplementary Movies 1, 2, and 3). Notably, the displacements were largely different between the days. Thus, the contractile force was calculated using the displacement. The time course trend of the contractile force is shown in Fig. 4D. The contractile force was 0.92 ± 0.18 μN on day 2 and slightly increased to 1.9 ± 0.052 μN on day 4. It largely increased to 18 ± 4.2 μN on day 5 and was maintained at 19 ± 1.7 μN on day 6. It then decreased to 0.25 ± 0.028 μN on day 8 and remained at 0.25 ± 0.023 μN on day 10.

As shown in Fig. 4D, the spontaneous contractile force of the cocultured tissues on the device reached the maximum value on day 6 and then decreased significantly on day 8. In addition, the periodicity was diminished on day 8 (Fig. 4C). To explore the reason for this trend, we measured the contractile force of the cocultured SkM tissues induced via electrical pulse stimulation (EPS) applied to the SkM chamber (Supplementary Fig. 3). By applying EPS to the SkM chamber, we could induce contraction in all the contractible myotubes in the SkM tissues. On day 6, the contractile force of EPS-induced contraction (20 ± 1.6 μN) was almost identical to that of the spontaneous contraction (19 ± 1.7 μN) (Fig. 4D and Supplementary Fig. 3). In contrast, on day 8, it was considerably higher (11 ± 2.1 μN for EPS-induced contraction and 0.25 ± 0.028 μN for

spontaneous contraction). Considering these results, it is suggested that the most of myotubes in the cocultured SkM tissues on day 6 synchronously contracted in response to the spontaneous firing of MNs, whereas the myotubes in the tissues contracted asynchronously on day 8. We speculate that the gap junction that enables the propagation of electrical activity between cells may play a key role in the synchronous contraction observed on day 6. During muscle development and regeneration *in vivo*, gap junctions are expressed transiently (39, 40). By *in vitro* experiments using 2D cultured rat primary myoblasts, Gorbe et al. reported that the permeability of gap junctions increased and decreased significantly in a few days after inducing differentiation (41). Considering these results, we assume that the myotubes within the cocultured tissue on day 6 contracted synchronously in response to the spontaneous firing of MNs due to calcium ion propagation through the highly expressed gap junctions and, as the expression decreased, the myotubes contracted without synchronization, leading to the small and nonperiodical contraction of the tissues.

To evaluate whether the cocultured SkM tissues were innervated by MNs, we applied shear stress to the middle of the axons using the microchannel for axon stimulation (# in Fig. 2C) and observed the effects on the contraction of the tissues. As expected, the spontaneous contraction of the cocultured SkM tissues due to the spontaneous firing of MNs disappeared upon the application of shear stress (Fig. 5). This result shows that the myotubes in the SkM tissues on day 10 formed functional NMJs with the terminal of the axons from MN spheroids. This also indicates the possibility of using the developed device to model SkM atrophy after a nerve injury.

3.4 Functional assessments of the compartmentalized 3D neuromuscular tissue models on the devices

We evaluated the functionality of compartmentalized neuromuscular tissue models fabricated on the device. We added the excitatory neurotransmitter glutamate into the MN chamber to induce the firing of the MNs and measured the displacement of the micropost due to the SkM tissue contraction. We used the cocultured tissues on day 10. To reduce the spontaneous firing of MNs, the cocultured tissues were incubated at 25 °C for 10 min before adding glutamate (Fig. 6A-i). When we added PBS (vehicle control) to the SkM chamber or MN chamber, no contraction of the SkM tissue was observed (data not shown). In contrast, as shown in Fig. 6A-ii, the addition of glutamate into the MN chamber induced a lasting contraction, or tetanus, of the tissues.

Subsequently, we added the sodium channel blocker, TTX, or antagonist to the nicotinic AChRs, Vb, into the MN chamber or SkM chamber, and evaluated their effects on the muscle contraction induced by glutamate (Fig. 6B and C). When TTX was added to the MN chamber, the muscle contraction did not occur, but muscle relaxation was observed (Fig. 6B-i). In contrast, when TTX was added to the SkM chamber, the muscle contraction was observed (Fig. 6B-ii). When Vb was added to the MN chamber, the muscle contraction was observed (Fig. 6C-i). In contrast, when Vb was added into the SkM chamber, the muscle contraction did not occur and muscle relaxation was observed (Fig. 6C-ii). The difference observed for TTX and Vb (Fig. 6B and C) could be explained by the inhibitory mechanisms of TTX and Vb. TTX blocks the voltage-gated sodium channels expressed in the MNs, while Vb binds to the nicotinic AChR expressed in the SkM cells. Considering these results, although further experiments for examining the effects of dose response and/or long-term exposure are needed, the developed compartmentalized neuromuscular tissue-on-a-chip models have the potential to evaluate the effects of cellular type specific drug candidates on the contractile force of SkM tissues.

As shown in Fig. 6A, the cocultured tissues on day 10 exhibited tetanic contraction by the addition of glutamate in the MN chamber. The previous 3D coculture models (8, 11, 14, 15) exhibited twitch contraction upon exposure to glutamate. Although the reason for the difference between the results of this study and previous studies is unclear, we believe that the maturation state of the SkM tissues in this study might be one of the reasons. Considering the precise compartmentalized nature of our device, the MNs and SkM tissues can be cultured in each specific culture medium, leading to the maturation of the SkM tissues. Furthermore, in this study, we used immortalized human myogenic cells, Hu5/KD3. In our previous study, we fabricated engineered Hu5/KD3 SkM tissues and showed that they generated a larger contractile force than that of the tissues engineered from other cell types, including C2C12, primary cells, and reprogrammed stem cells (31, 32). This result suggests that the maturation of Hu5/KD3 tissues was more advanced than those of C2C12 (8, 11, 14) or reprogrammed stem cells (15) used in other studies. Further experiments will be performed to understand the mechanisms underlying this phenomenon in the future.

4. Conclusion

In this study, we developed a microdevice for precisely compartmentalized coculturing of MNs and engineered SkM tissues. Our data suggest that the developed device has the following characteristics. First, it is possible to measure the force of engineered SkM tissues whose contraction is induced by MNs through NMJs. Second, it is possible to compartmentalize the cell bodies of MNs and SkM cells during a culture period. Third, it is possible to apply chemical/mechanical stimuli to the cell bodies of MNs and SkM cells and middle of the axons. Thus, the microdevice would be a useful tool in fundamental research and drug development for neuromuscular disorders.

Acknowledgments

We thank Dr. Naohiro Hashimoto at the National Center for Geriatrics and Gerontology for providing Hu5/KD3 cells. This research was supported in part by Japan Society for the Promotion of Science KAKENHI Grant Numbers 26630429, JP16KK0126, JP18H01796, and JP20H04705. We would like to thank Editage for the English language editing.

References

1. Witzemann V. Development of the neuromuscular junction. Cell Tissue Res. 2006;326(2):263-71.

2. Darabid H, Perez-Gonzalez AP, Robitaille R. Neuromuscular synaptogenesis: coordinating partners with multiple functions. Nature Reviews Neuroscience. 2014;15(11):703-18.

3. Bhatt JM. The Epidemiology of Neuromuscular Diseases. Neurol Clin. 2016;34(4):999-1021.

4. Santoso JW, McCain ML. Neuromuscular disease modeling on a chip. Disease Models & Mechanisms. 2020;13(7):dmm044867.

5. Vila OF, Qu Y, Vunjak-Novakovic G. In vitro models of neuromuscular junctions and their potential for novel drug discovery and development. Expert Opin Drug Discov. 2020;15(3):307-17.

6. Natarajan A, Sethumadhavan A, Krishnan UM. Toward Building the Neuromuscular Junction: In Vitro Models To Study Synaptogenesis and Neurodegeneration. ACS Omega. 2019;4(7):12969-77.

7. Badiola-Mateos M, Hervera A, Del Río JA, Samitier J. Challenges and Future Prospects on 3D in-vitro Modeling of the Neuromuscular Circuit. Frontiers in bioengineering and biotechnology. 2018;6:194-.

8. Morimoto Y, Kato-Negishi M, Onoe H, Takeuchi S. Three-dimensional neuron-muscle constructs with neuromuscular junctions. Biomaterials. 2013;34(37):9413-9.

9. Martin NR, Passey SL, Player DJ, Mudera V, Baar K, Greensmith L, et al. Neuromuscular Junction Formation in Tissue-Engineered Skeletal Muscle Augments Contractile Function and Improves Cytoskeletal Organization. Tissue Eng Part A. 2015;21(19-20):2595-604.

10. Smith AS, Passey SL, Martin NR, Player DJ, Mudera V, Greensmith L, et al. Creating Interactions between Tissue-Engineered Skeletal Muscle and the Peripheral Nervous System. Cells Tissues Organs. 2016;202(3-4):143-58.

11. Cvetkovic C, Rich MH, Raman R, Kong H, Bashir R. A 3D-printed platform for modular neuromuscular motor units. Microsystems & Nanoengineering. 2017;3:17015.

12. Maffioletti SM, Sarcar S, Henderson ABH, Mannhardt I, Pinton L, Moyle LA, et al. Three-Dimensional Human iPSC-Derived Artificial Skeletal Muscles Model Muscular Dystrophies and Enable Multilineage Tissue Engineering. Cell Reports. 2018;23(3):899-908.

13. Afshar Bakooshli M, Lippmann ES, Mulcahy B, Iyer N, Nguyen CT, Tung K, et al. A 3D culture model of innervated human skeletal muscle enables studies of the adult neuromuscular junction. eLife. 2019;8:e44530.

14. Uzel SGM, Platt RJ, Subramanian V, Pearl TM, Rowlands CJ, Chan V, et al. Microfluidic device for the formation of optically excitable, three-dimensional, compartmentalized motor units. Science Advances. 2016;2:e1501429.

15. Osaki T, Uzel SGM, Kamm RD. Microphysiological 3D model of amyotrophic lateral sclerosis (ALS) from human iPS-derived muscle cells and optogenetic motor neurons. Sci Adv. 2018;4(10):eaat5847.

16. Vila OF, Uzel SGM, Ma SP, Williams D, Pak J, Kamm RD, et al. Quantification of human neuromuscular function through optogenetics. Theranostics. 2019;9(5):1232-46.

17. Aydin O, Passaro AP, Elhebeary M, Pagan-Diaz GJ, Fan A, Nuethong S, et al. Development of 3D neuromuscular bioactuators. APL Bioengineering. 2020;4(1):016107.

18. Campenot RB. Local Control of Neurite Development by Nerve Growth-Factor. Proc Natl Acad Sci U S A. 1977;74(10):4516-9.

19. Taylor AM, Blurton-Jones M, Rhee SW, Cribbs DH, Cotman CW, Jeon NL. A microfluidic culture platform for CNS axonal injury, regeneration and transport. Nat Methods. 2005;2(8):599-605.

20. Southam KA, King AE, Blizzard CA, McCormack GH, Dickson TC. Microfluidic primary culture model of the lower motor neuron-neuromuscular junction circuit. J Neurosci Methods. 2013;218(2):164-9.

21. Tong Z, Seira O, Casas C, Reginensi D, Homs-Corbera A, Samitier J, et al. Engineering a functional neuro-muscular junction model in a chip. Rsc Advances. 2014;4(97):54788-97.

22. Yamaoka N, Shimizu K, Imaizumi Y, Ito T, Okada Y, Honda H. Open-Chamber Co-Culture Microdevices for Single-Cell Analysis of Skeletal Muscle Myotubes and Motor Neurons with Neuromuscular Junctions. Biochip Journal. 2019;13(2):127-32.

23. Machado CB, Pluchon P, Harley P, Rigby M, Sabater VG, Stevenson DC, et al. In Vitro Modeling of Nerve-Muscle Connectivity in a Compartmentalized Tissue Culture Device. Adv Biosyst. 2019;3(7).

24. Zahavi EE, Ionescu A, Gluska S, Gradus T, Ben-Yaakov K, Perlson E. A compartmentalized microfluidic neuromuscular co-culture system reveals spatial aspects of GDNF functions. J Cell Sci. 2015;128(6):1241-52.

25. Santhanam N, Kumanchik L, Guo X, Sommerhage F, Cai Y, Jackson M, et al. Stem cell derived phenotypic human neuromuscular junction model for dose response evaluation of therapeutics. Biomaterials. 2018;166:64-78.

26. Kilinc D, Peyrin J-M, Soubeyre V, Magnifico S, Saias L, Viovy J-L, et al. Wallerian-Like Degeneration of Central Neurons After Synchronized and Geometrically Registered Mass Axotomy in a Three-Compartmental Microfluidic Chip. Neurotoxicity Research. 2011;19(1):149-61.

27. Shimizu K, Fujita H, Nagamori E. Evaluation systems of generated forces of skeletal muscle cell-based bio-actuators. Journal of Bioscience and Bioengineering. 2013;115(2):115-21.

28. Madden L, Juhas M, Kraus WE, Truskey GA, Bursac N. Bioengineered human myobundles mimic clinical responses of skeletal muscle to drugs. eLife. 2015;4:e04885.

29. Nesmith AP, Wagner MA, Pasqualini FS, O'Connor BB, Pincus MJ, August PR, et al. A human in vitro model of Duchenne muscular dystrophy muscle formation and contractility. J Cell Biol. 2016;215(1):47-56.

30. Shimizu K, Genma R, Gotou Y, Nagasaka S, Honda H. Three-Dimensional Culture Model of Skeletal Muscle Tissue with Atrophy Induced by Dexamethasone. Bioengineering (Basel). 2017;4(2):56.

31. Shimizu K, Ohsumi S, Kishida T, Mazda O, Honda H. Fabrication of contractile skeletal muscle tissues using directly converted myoblasts from human fibroblasts. J Biosci Bioeng. 2020;129(5):632-7.

32. Nagashima T, Hadiwidjaja S, Ohsumi S, Murata A, Hisada T, Kato R, et al. In Vitro Model of Human Skeletal Muscle Tissues with Contractility Fabricated by Immortalized Human Myogenic Cells. Adv Biosyst. 2020:e2000121.

33. Takahashi K, Tanabe K, Ohnuki M, Narita M, Ichisaka T, Tomoda K, et al. Induction of pluripotent stem cells from adult human fibroblasts by defined factors. Cell. 2007;131(5):861-72.

34. Nagashima T, Shimizu K, Matsumoto R, Honda H. Selective Elimination of Human Induced Pluripotent Stem Cells Using Medium with High Concentration of L-Alanine. Sci Rep. 2018;8(1):12427.

35. Shimojo D, Onodera K, Doi-Torii Y, Ishihara Y, Hattori C, Miwa Y, et al. Rapid, efficient, and simple motor neuron differentiation from human pluripotent stem cells. Molecular Brain. 2015;8:79.

36. Shiomi K, Kiyono T, Okamura K, Uezumi M, Goto Y, Yasumoto S, et al. CDK4 and cyclin D1 allow human myogenic cells to recapture growth property without compromising differentiation potential. Gene Ther. 2011;18(9):857-66.

37. Kawada J, Kaneda S, Kirihara T, Maroof A, Levi T, Eggan K, et al. Generation of a Motor Nerve Organoid with Human Stem Cell-Derived Neurons. Stem Cell Rep. 2017;9(5):1441-9.

38. Ko E, Yu SJ, Pagan-Diaz GJ, Mahmassani Z, Boppart MD, Im SG, et al. Matrix Topography Regulates Synaptic Transmission at the Neuromuscular Junction. Advanced Science. 2019;6(6):1801521.

39. Constantin B, Cronier L. Involvement of gap junctional communication in myogenesis. Int Rev Cytol. 2000;196:1-65.

40. Araya R, Eckardt D, Maxeiner S, Krüger O, Theis M, Willecke K, et al. Expression of connexins during differentiation and regeneration of skeletal muscle: functional relevance of connexin43. J Cell Sci. 2005;118(1):27-37.

41. Gorbe A, Becker DL, Dux L, Krenacs L, Krenacs T. In differentiating prefusion myoblasts connexin43 gap junction coupling is upregulated before myoblast alignment then reduced in post-mitotic cells. Histochemistry and Cell Biology. 2005;125(6):705.

Figure legends

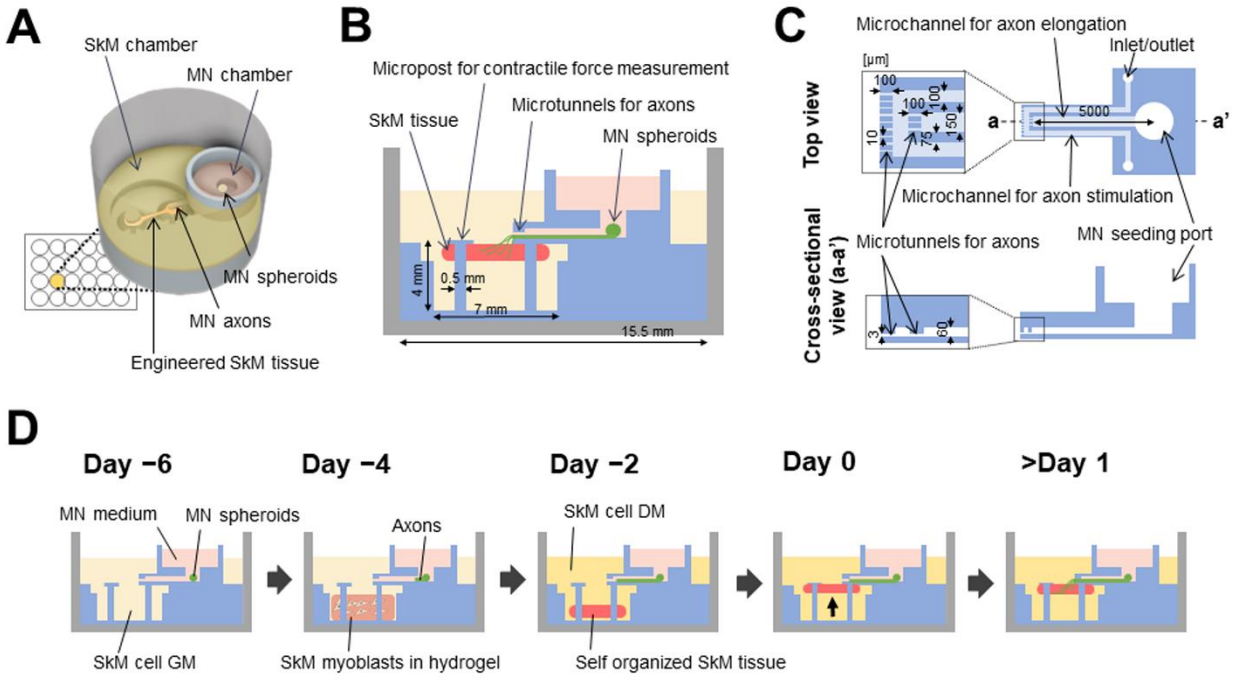

Fig. 1 Schematic of the 24-well-format microdevice. A) Single view of the device. B) Cross-sectional view. C) Chamber for MNs. D) Scheme for coculture on the microdevices.

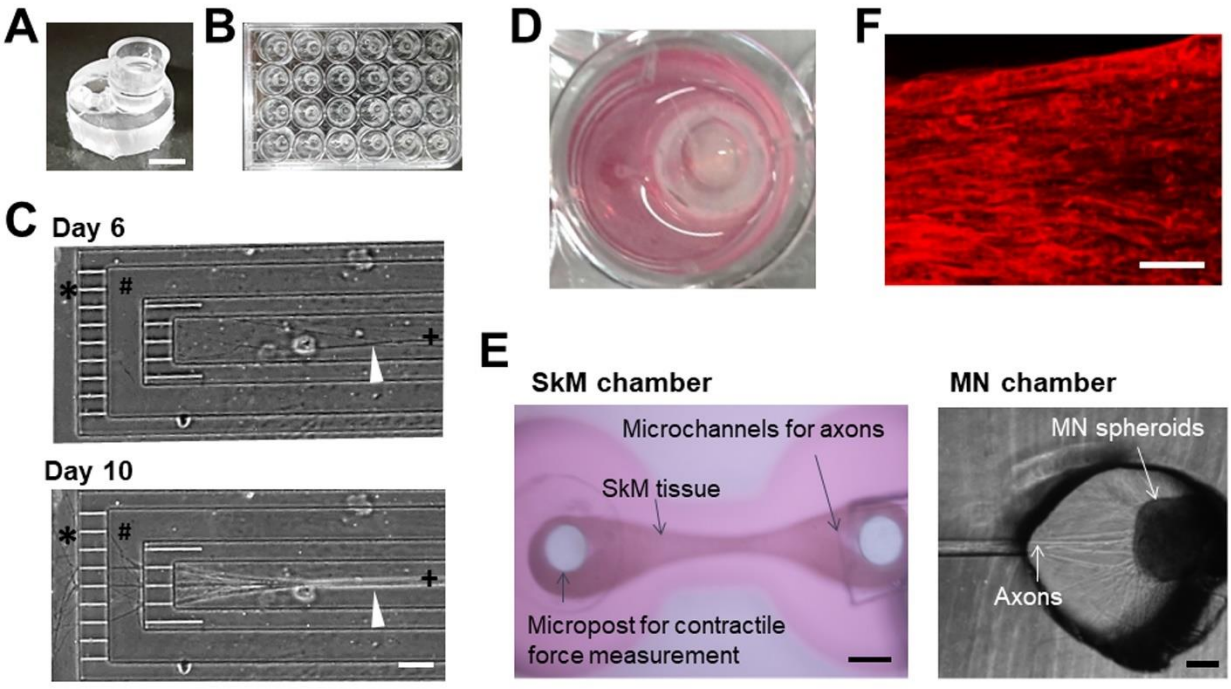

Fig. 2 Fabrication and use of the microdevice. A) Image of fabricated microdevice. Scale bar: 5 mm. B) Image of the 24-well plate with the microdevices. C) Axon elongation in the MN chamber. Representative image of elongated axons from the MN spheroid on day 6 and day 10. Axons from the MN spheroid elongate in the MN chamber (+) and reach the outside space (*). The gap between the microtunnels for axons (#) is used as a microchannel for axon stimulation. Arrow head: elongated axons. Scale bar: 100 μm. D) Image of one well of the 24-well plate with the device with SkM tissues and MNs. E) Image of SkM tissue on the device. Scale bar: 500 μm. F) Fluorescence micrograph of myotubes in SkM tissue. Scale bar: 100 μm.

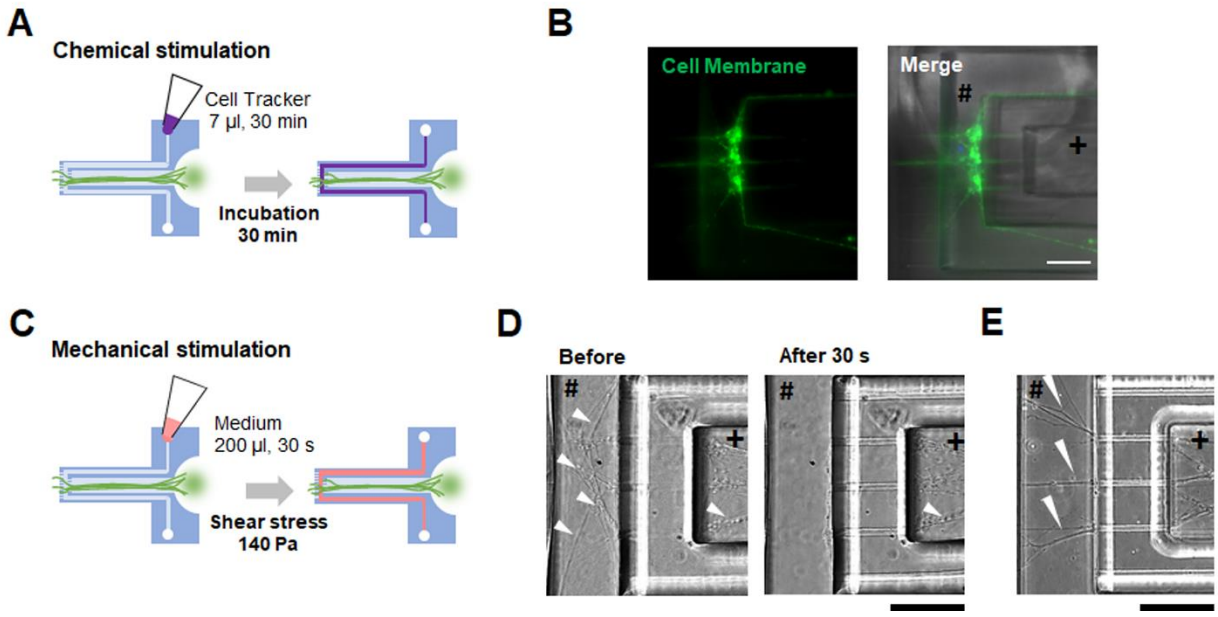

Fig. 3 Selective stimulation of the middle of the axons. A) Scheme for chemical stimulation. B) Selective fluorescent labeled axons in the microchannel for axon stimulation (#). Scale bar: 100 µm. C) Scheme for mechanical stimulation. D) Selective removal of the axons in the microchannel for axon stimulation (#) via shear stress. Scale bar: 100 µm. E) Re-elongation of axons in the microchannels for axon stimulation (#). Scale bar: 100 µm.

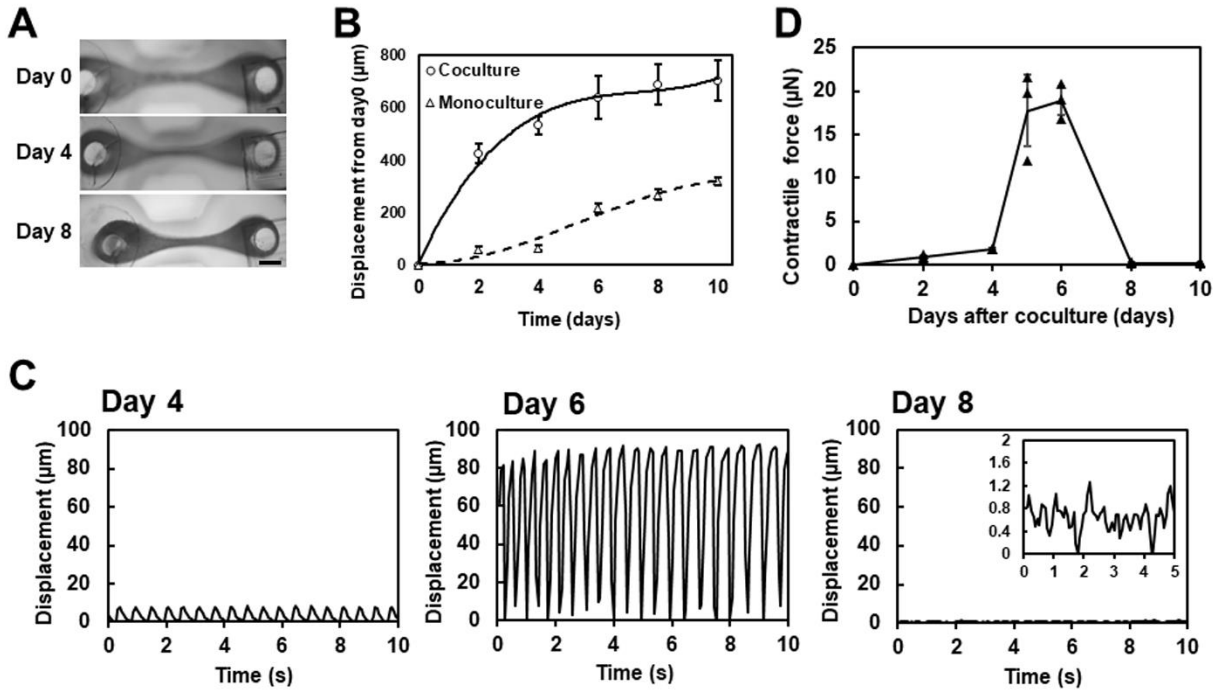

Fig. 4 Coculture of MN spheroids and engineered SkM tissues on the device. A) Representative images of SkM tissues on the device on day 0, 4, and 8. Scale bar: 500 μm. B) Displacement of the micropost by passive tension of the cocultured tissues. Open circle: with MN spheroids. Open triangle: without MN spheroids. C) Displacement of micropost moved by contraction of SkM tissues, which was generated in response to spontaneous firing of MNs on day 4, 6, and 8. D) Quantified contractile force of SkM tissues cocultured with MNs on the devices.

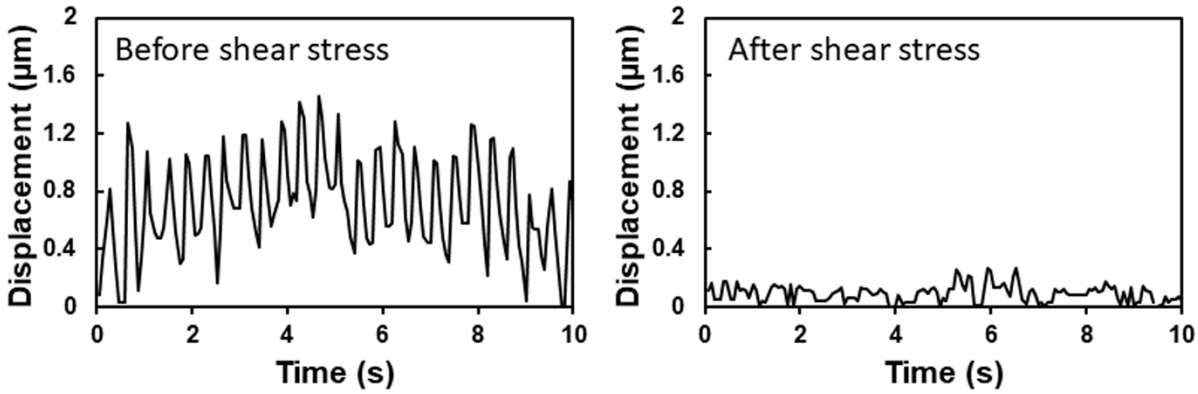

Fig. 5 Application of shear stress to the middle of the axon of cocultured tissues on day 10. Representative results are displayed (n=3).

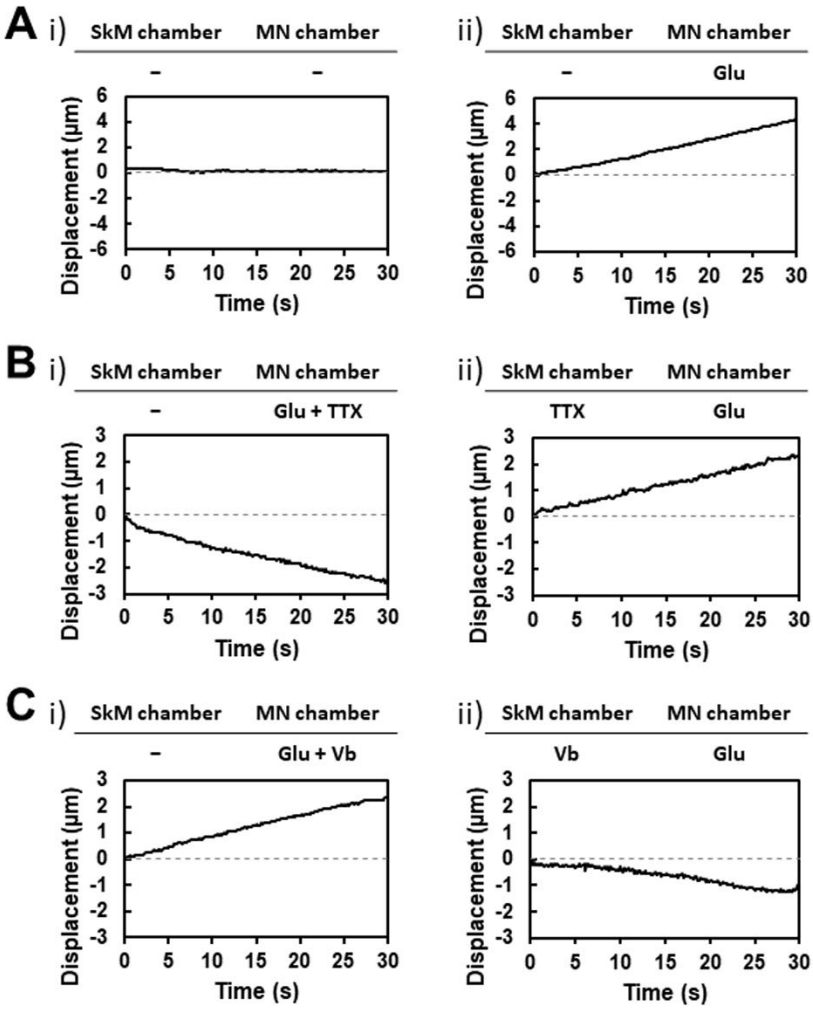

Fig. 6 Assessment of functionality of the cocultured tissues on the devices. A) Displacement of micropost after the addition of glutamate (Glu) in the MN chamber. Representative results are displayed (n=3). B) Displacement of micropost after the addition of TTX in the SkM or MN chamber. Glutamate was added to the MN chamber before the addition of TTX in each chamber. Representative results are displayed (n=2). C) Displacement of micropost after the addition of Vb in the SkM or MN chamber. Glutamate was added to the MN chamber before the addition of Vb in each chamber. Representative results are displayed (n=2).

Supplementary Figures

Supplementary Fig. 1 Fabrication process for the microdevice

Supplementary Fig. 2 Axon elongation in the MN chamber with one step nine microtunnels for axons. Scale bar: 100 μm.

Supplementary Fig.3 EPS-induced contractile force of cocultured SkM tissues on day 6 and 8. EPS (30 Hz, 2 ms, 5 V/mm) was applied to the SkM chamber. The displacement of the micropost during the EPS was measured and the contractile force was calculated.

Supplementary Movies

Supplementary Movies 1 The movement of the tip of the micropost due to the spontaneous contraction of the cocultured SkM tissue on day 4.

Supplementary Movies 2 The movement of the tip of the micropost due to the spontaneous contraction of the cocultured SkM tissue on day 6.

Supplementary Movies 3 The movement of the tip of the micropost due to the spontaneous contraction of the cocultured SkM tissue on day 8.